Fig. S1 (related to Fig. 1) - Bosch et al.

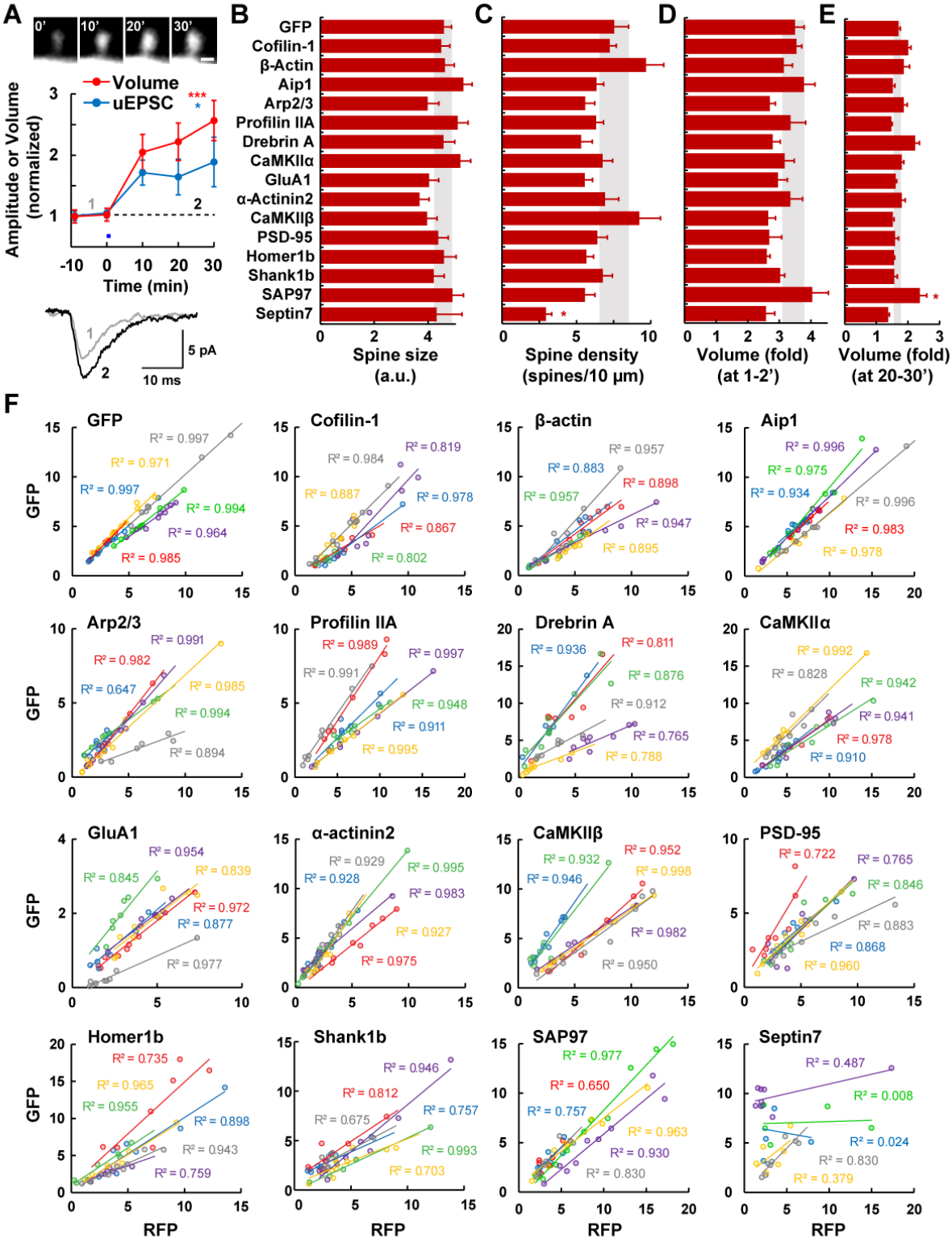

Fig. S2 (related to Fig. 2) - Bosch et al.

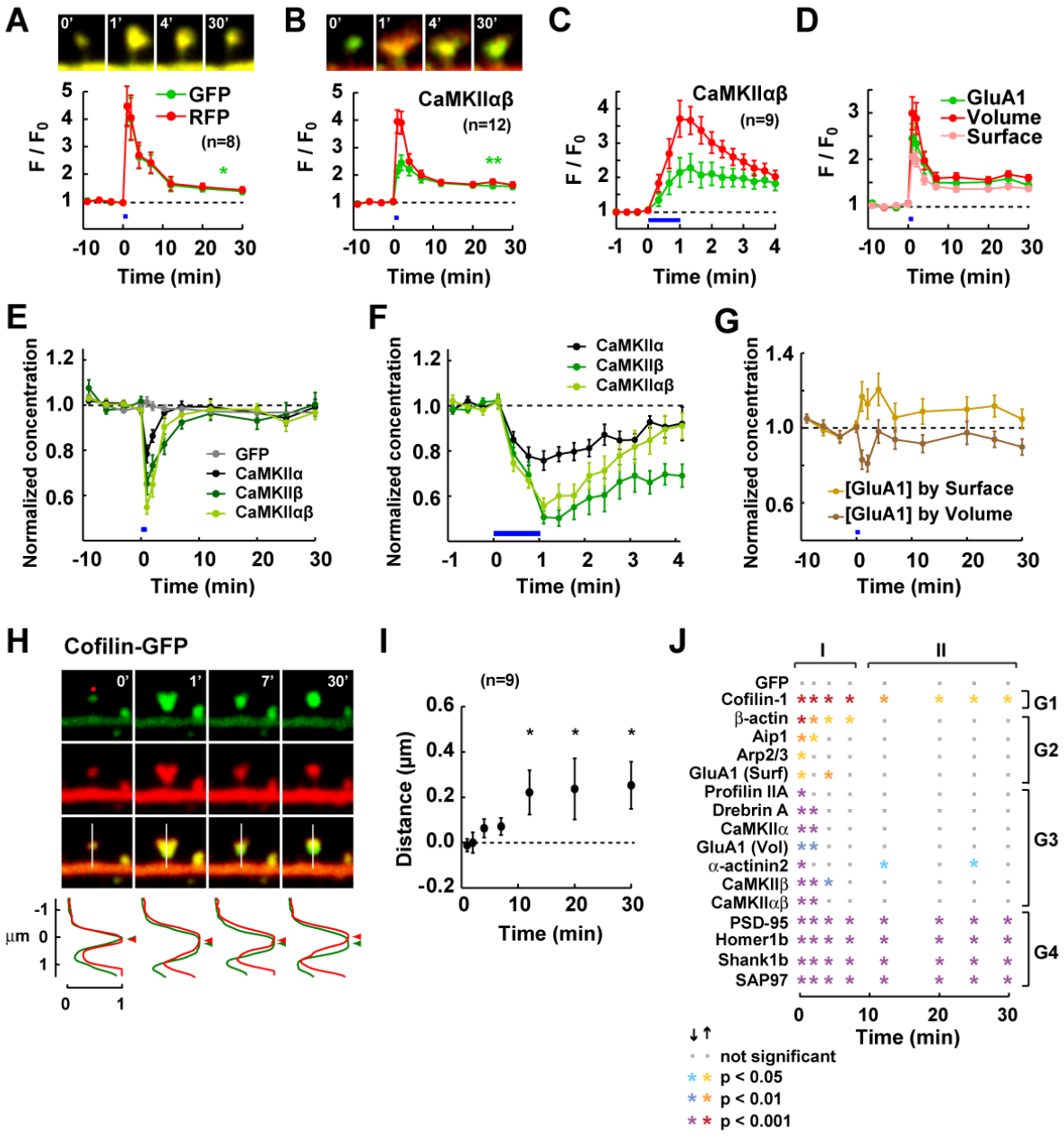

Fig. S3 (related to Fig. 3) - Bosch et al.

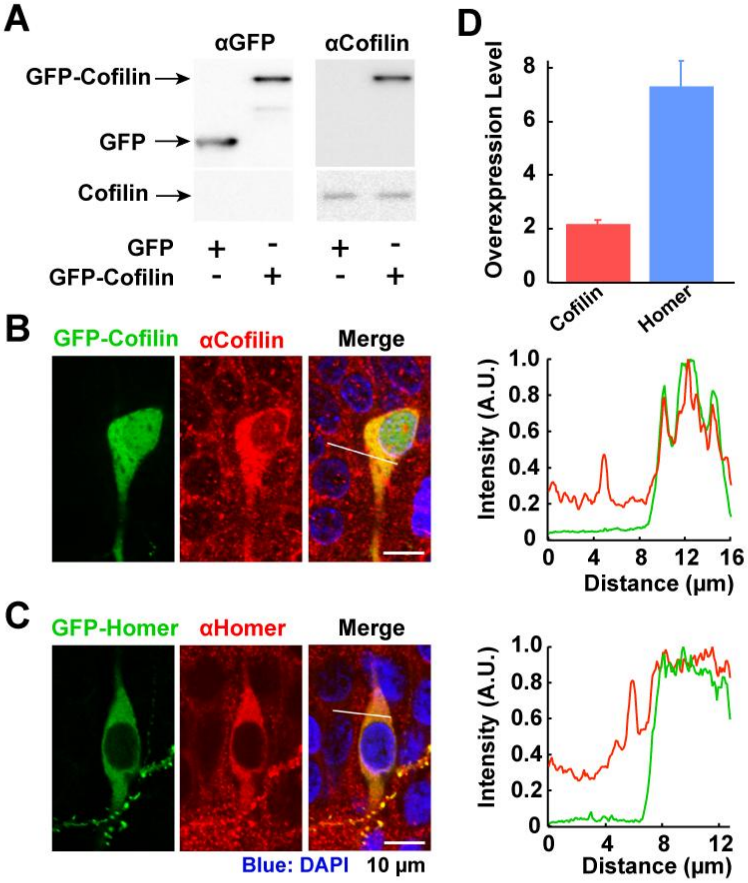

Fig. S4 (related to Fig. 5) - Bosch et al.

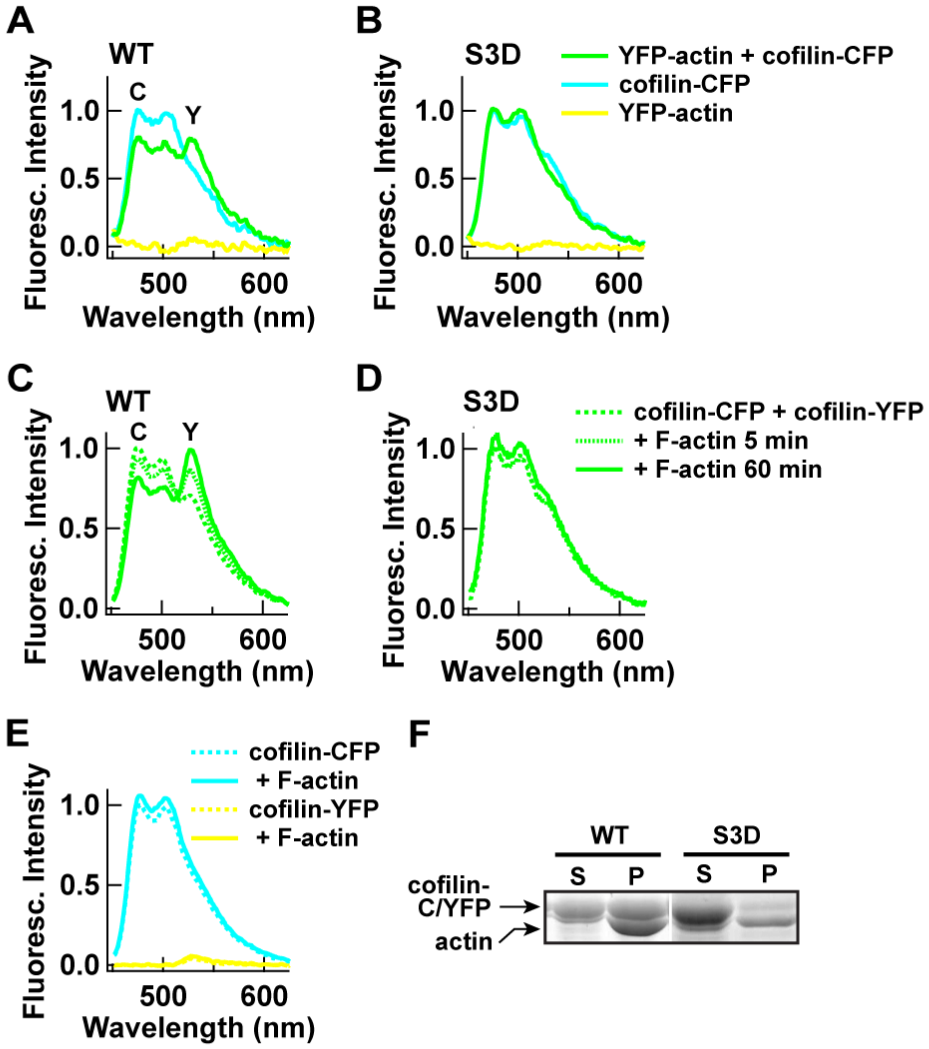

Fig. S5 (related to Fig. 6) - Bosch et al.

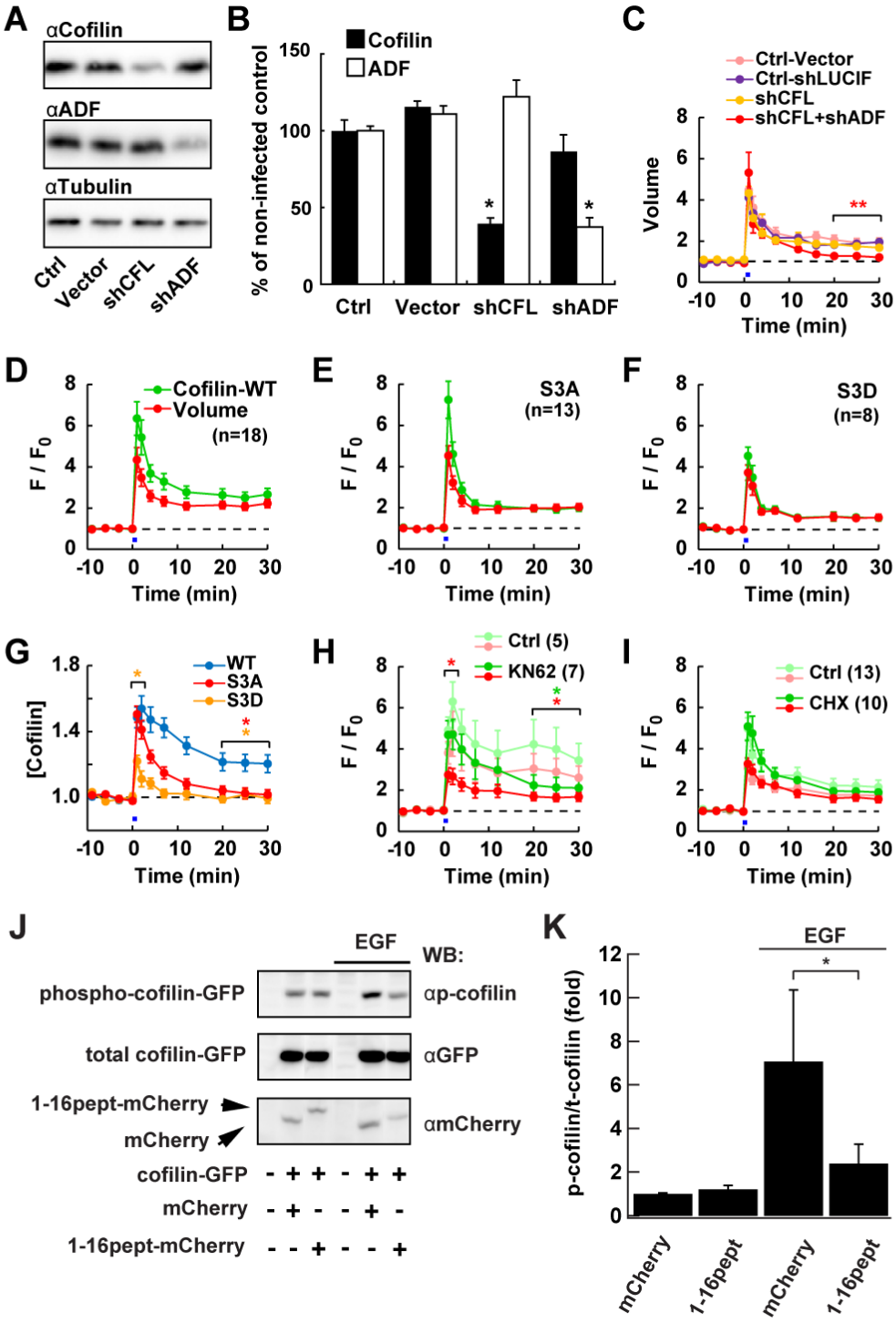

Fig. S6 (related to Fig. 8) - Bosch et al.

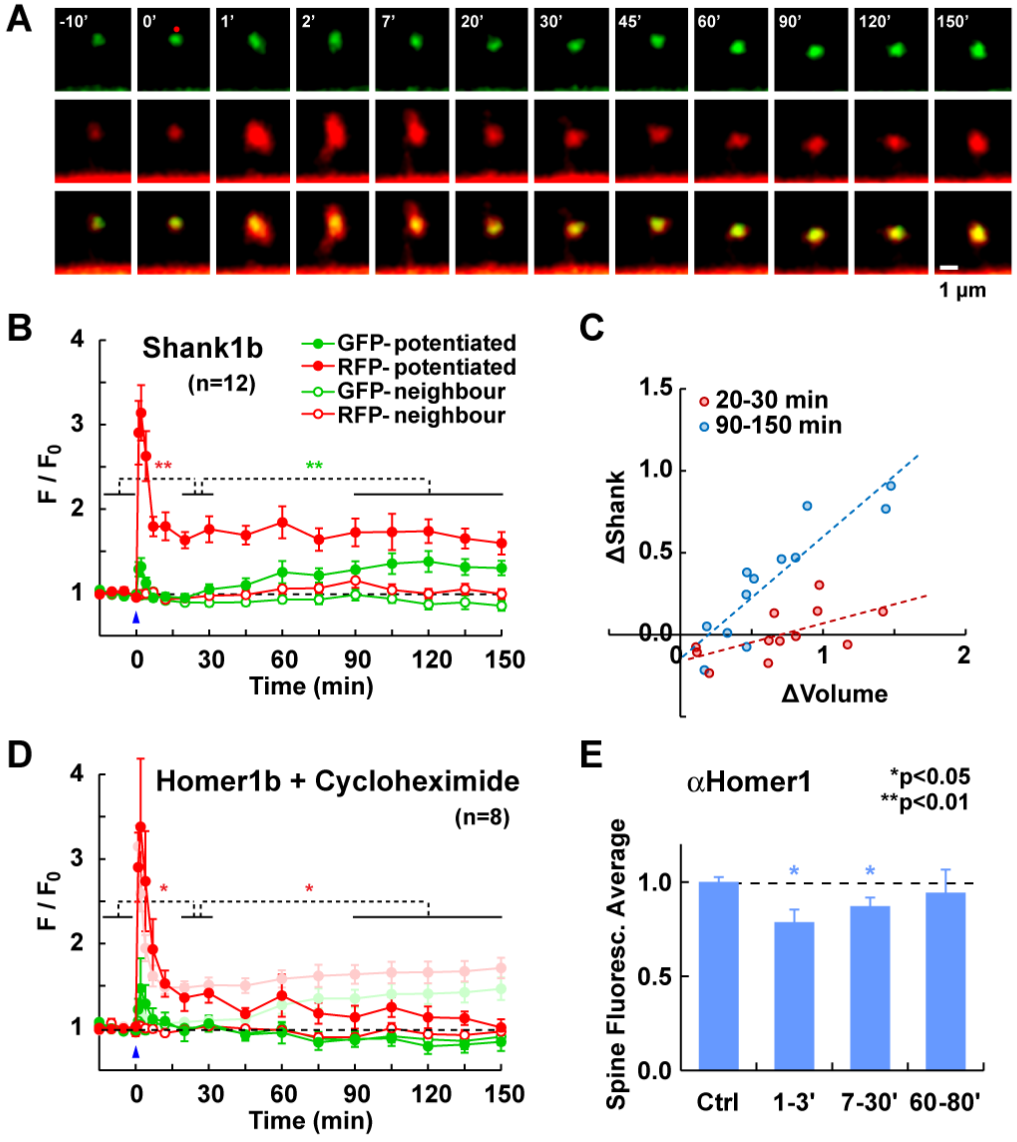

LEGENDS FOR SUPPLEMENTAL FIGURES

Fig. S1 (related to Fig. 1). Characterization of spine morphology and plasticity, and postsynaptic protein composition after expression of GFP-fusion proteins.

(A) Single-spine 2-photon glutamate uncaging evokes enlargement of dendritic spines in parallel with LTP of AMPAR-mediated synaptic responses. Amplitude of uncaging-evoked excitatory postsynaptic currents (uEPSC) and spine volume are normalized to baseline (mean ± SEM; n=9). * $p<0.05$, *** $p<0.001$ at 20-30 min after sLTP with respect to baseline. Sample traces (1 = baseline; 2 = 20-30 min) and images (scale bar: 0.5 μm; time stamp in min) are shown. See supplemental experimental procedures for statistical analysis.

(B-C) Expression of GFP-fusion proteins do not alter spine morphology or structural plasticity, except for septin 7, which shows a reduced spine density, and SAP97, which displays an enhanced persistent spine expansion. **(B)** Comparison of basal spine size (RFP fluorescence intensity, in arbitrary units) among neurons transfected with free GFP or any of the GFP-fusion proteins used in this study (44-50 spines analyzed per protein; 28 for septin). **(C)** A similar comparison of spine density (10-22 dendritic segments analyzed; 5 for septin).

(D-E) A similar comparison for the magnitude (fold over baseline) of spine enlargement at the 1-2 min **(D)** and 20-30 min **(E)** interval after induction of sLTP (number of spines analyzed is the same as in **Fig. 1** except for GFP [n=20], cofilin [n=54] and Homer1b [n=47]). * $p<0.05$ with respect to GFP-transfected cells.

(F) The amount of postsynaptic protein in the spine head is proportional to the spine volume. Each panel plots the RFP fluorescence intensity (proportional to the spine volume) versus the GFP fluorescence intensity (proportional to the total amount of the GFP-fusion protein) in the

spine head, in arbitrary units. For septin 7, GFP intensity is measured from the cluster in the dendritic shaft closest to each spine. As every neuron may have different relative GFP and RFP expression levels, every neuron (n=6 neurons; 4-10 spines/neuron) is plotted separately in a different color with its own linear regression line. Note the strong correlation between the volume of the spine and the amount of protein in the spine head, for all proteins except for septin 7.

Fig. S2 (related to Fig. 2). Dynamics of GFP, CaMKIIα+β heteroligomer and surface GluA1 in dendritic spines, subspine redistribution of cofilin during sLTP, and statistical analysis.

(A-C) Time course of unfused free GFP **(A)** or GFP-CaMKIIα + untagged CaMKIIβ **(B-C)** fluorescence intensity (F; normalized to baseline F_0) in the spine (RFP as volume marker) during 30 min **(A-B)** or 4 min **(C)** after sLTP induction (mean ± SEM). Time-lapse images are 3 μm wide. * $p<0.05$, ** $p<0.01$ between protein amount at 20-30 min and at baseline.

(D) Time course of GluA1 amount, spine volume (same data as in **Fig. 1A**) and spine surface area (calculated as the 2/3 power of the hypothetical spherical volume) after sLTP induction.

(E-G) Relative protein concentration in the spine (GFP/RFP ratio, normalized to baseline) during 30 min **(E, G)** or 4 min **(F)** after sLTP induction. **(E-F)** Changes in concentration of free GFP, GFP-CaMKIIα, GFP-CaMKIIβ (data from **Fig. 2A-B**), and GFP-CaMKIIα + untagged CaMKIIβ heteroligomer. **(G)** Comparison of GluA1 concentration [GluA1], calculated by dividing GluA1 amount by the entire spine volume (as in **Fig. 2A**), or surface GluA1 density by dividing GluA1 amount by the spine surface area.

(H-I) Subspine redistribution of cofilin-GFP after sLTP induction. **(H)** Fluorescence profile of cofilin-GFP and RFP across a longitudinal axis perpendicular to the dendritic shaft (white line), normalized to the peak value in the spine (marked by arrowheads), at different time points after induction of sLTP. **(I)** Average distance between the position of the GFP and RFP peaks, indicating how far cofilin-GFP is from the center of the spine head. * $p<0.05$ with respect to 1 min after sLTP.

(J) Statistical analysis of the significant differences in protein concentration at each time point in **Fig. 2A, S2E, S2G** with respect to its baseline before LTP induction (by repeated measures ANOVA followed by Dunnett's *post hoc* test). The transition from Phase I to Phase II (7 min) is set at the time point were all G2-G3 proteins were no longer significantly different with respect to the baseline (with the exception of α-actinin2). GluA1 can be classified as G3 protein if concentration is calculated by volume (Vol) or as G2 protein if calculated by surface area (Surf).

Fig. S3 (related to Fig. 3). Levels of overexpression of GFP-cofilin and GFP-Homer1b.

(A) Validation of the antibody used to detect cofilin-1 in western blot of HEK293 cells expressing GFP or GFP-cofilin.

(B) Detection of endogenous cofilin and exogenous GFP-cofilin by immunohistochemistry in neurons expressing GFP-cofilin in slice culture. Fluorescence intensity profiles (in arbitrary units) across a neuron expressing GFP-cofilin and non-transfected adjacent cells (white line) are shown on the right. Green, anti-GFP channel; red, anti-cofilin channel.

(C) A similar immunostaining experiment with Homer.

(D) Quantification of levels of overexpression of GFP-cofilin (mean ± SEM; n=12 transfected cells, each of which was compared with 3 untransfected cells in the same image) and GFP-Homer1b (n=10 transfected cells, each compared with 3 untransfected cells).

Fig. S4 (related to Fig. 5). Confirmation of FRET between actin and cofilin *in vitro*.

(A, B) FRET between YFP-actin and cofilin-CFP. Emission spectra of a solution containing polymerized YFP-actin and cofilin-CFP (either wild type (WT) **(A)** or S3D mutant **(B)**), cofilin-CFP (WT or S3D) only, and YFP-actin only, at CFP specific excitation of 400 ± 7.5 nm. Peak positions of CFP (C) and YFP emission (Y) are shown in **A**.

(C) FRET between cofilin-CFP and cofilin-YFP. Emission spectra of mixture of cofilin-CFP and cofilin-YFP before, 5 min and 60 min after addition of F-actin are shown.

(D) A similar experiment using mixture of cofilin S3D mutant-CFP and -YFP before and after the addition of F-actin.

(E) A similar experiment using cofilin-CFP or cofilin-YFP, with and without F-actin.

(F) A biochemical demonstration of binding between F-actin and cofilin. Note that WT but not S3D cofilin co-sediment with actin. S: supernatant, P: pellet.

Fig. S5 (related to Fig. 6). Function and mechanism of activity-dependent translocation and retention of cofilin into the spine during sLTP.

(A-B) Efficiency of shRNAs against cofilin and ADF. **(A)** Fourteen days *in vitro* (DIV) dissociated hippocampal neurons were infected with lentivirus carrying shRNA against cofilin (shCFL) or ADF (shADF). After 6 days, neurons were lysed, separated on SDS-PAGE and blotted with anti-cofilin (αCFL), anti-ADF (αADF) and anti-Tubulin (αTubulin) antibodies. **(B)**

Quantification of the amount of cofilin and ADF (mean ± SEM; n=5), normalized to control conditions. Ctrl, no infection; Vector, empty viral vector. * $p<0.05$ with respect to Ctrl.

(C) shRNA against cofilin alone (shCFL) is not sufficient to block the persistent spine enlargement after LTP induction. Time-course of spine volume after sLTP in the presence of empty shRNA vector (Ctrl-Vector; same data as in **Fig. 6B**), shRNA against Luciferase (shLUCIF) as an additional control, shCFL+shADF (same data as in **Fig. 6B**; ** $p<0.01$ with respect to both controls), and shCFL alone.

(D-F) Time course of spine volume (red lines) and spine amount of cofilin-GFP (green lines) wildtype **(D)**, S3A **(E)**, and S3D **(F)** mutants during sLTP in the absence of shRNAs against cofilin and ADF.

(G) Time course of the relative spine concentration (GFP/RFP ratio) of cofilin wildtype, S3A, and S3D mutants. Under these conditions, sLTP is not impaired due to the presence of endogenous cofilin and ADF but translocation of mutants is impaired. * $p<0.05$ with respect to wildtype.

(H) A similar experiment to **Fig. 6L** using KN-62, a structurally distinct inhibitor of CaM kinase family. * $p<0.05$ with respect to no drug control. Number of experiments in parenthesis.

(I) Effect of protein synthesis blockade with cycloheximide (CHX) on the translocation of cofilin.

(J-K) Effect of 1-16 peptide on cofilin phosphorylation. (**J**) HeLa cells were cotransfected with cofilin-GFP and either cofilin peptide 1-16-mCherry (1-16pept-mCherry) or mCherry. Cells were stimulated with epidermal growth factor (EGF; 5 min). Phosphorylation of cofilin-GFP at Ser3 was determined by western blotting (WB) with phospho-cofilin antibody (αp-cofilin). (**K**) Quantification of cofilin-GFP phosphorylation. The ratio of phosphorylated cofilin-GFP (p-

cofilin) to the total amount of cofilin-GFP (t-cofilin) in the control (mCherry) is set to 1, and relative values are expressed as magnitude (fold) over 1 (n=6). *p< 0.05.

Fig. S6 (related to Fig. 8). Protein synthesis-dependent late synaptic translocation of Homer1b and Shank1b.

(A) Time-lapse images of a potentiated spine (red dot) expressing GFP-Shank1b and RFP. Time stamp in min.

(B) Time course of the amount of GFP-Shank1b in the spine head and the volume of the spine (RFP) after sLTP induction (mean ± SEM).

(C) Correlation between changes in Shank1b amount versus changes in spine volume in the same set of spines at 20-30 min (red) and at 90-150 min (blue) after sLTP induction.

(D) The delayed increase in the spine amount of GFP-Homer1b is blocked by the translational blocker cycloheximide. The no-drug control data from **Fig. 8B** are shown in faint colors for comparison.

(E) Immunostaining of endogenous Homer1 (αHomer1) confirms the delayed increase in the spine amount of Homer1. Quantification of the spine protein concentration measured as the average immunofluorescence (spine head intensity divided by spine head area) of potentiated spines at three time periods (1-3 min, n=7; 7-30 min, n=25 [same data as in **Fig 3C**]; and 60-80 min after sLTP, n=10) normalized to unstimulated spines (Ctrl, n=118) from the same optical section. * significant difference with respect to Ctrl.

Supplemental Table S1 (related to Fig. 1). Fusion protein cDNAs used in this study.

Name of protein	**Origin**	**Type of fluorescent protein**	**Position of fluorescent protein**	**Promoter**	**Source (researcher/affiliation/reference)**	**References on protein synaptic distribution and function**
β-actin	human	EGFP, mRFP	N-terminus N-terminus	CMV CAG	Clontech Takeo Saneyoshi and Thomas Soderling (Vollum Institute) (Saneyoshi et al., 2008)	(Fischer et al., 1998; Okamoto et al., 2004)
Non-muscle cofilin (cofilin-1)	mouse	EGFP PAGFP, mCherry	C-terminus C-terminus C-terminus	CMV CMV CMV	In house In house In house	(Gu et al., 2010)
AIP1 (WDR1)	mouse	EGFP	C-terminus	CAG	In house	
Cofilin 1-16 peptide	mouse	mCherry	C-terminus	CAG	In house	(Aizawa et al., 2001; Gu et al., 2010)
p21 subunit of Arp2/3 complex	human	EGFP	C-terminus	CMV	Laura Machesky (Glasgow University) (Johnston et al., 2008)	(Maldonado, 2010)

Profilin IIA	mouse	EGFP	N-terminus	CMV	Walter Witke (EMBL) (Di Nardo et al., 2000) and Miguel Morales (Center for Biomedical Research of La Rioja) (Syriani et al., 2008)	(Ackermann and Matus, 2003)
Septin 7	rat	EGFP	N-terminus	Chicken β-actin	Makoto Kinoshita (Nagoya University) (Tada et al., 2007)	(Tada et al., 2007)
GluA1	rat	Super-ecliptic pHluorin (SEP)	Three amino acids downstream from signal peptide cleavage site	CAG	Roberto Malinow (UCSD) (Kopec et al., 2006)	(Shi et al., 1999; Makino and Malinow, 2009; Patterson et al., 2010)
CaMKIIα	rat	EGFP, PAGFP	N-terminus N-terminus	CMV CMV	In house (Okamoto et al., 2004) In house	(Shen et al., 1998; Okamoto et al., 2004; Asrican et al., 2007; Zhang et al., 2008)
CaMKIIβ	rat	mGFP [1)]	N-terminus	CMV	In house (Okamoto et al., 2004)	(Shen et al., 1998; Okamoto et al., 2004; Asrican et al., 2007)
Drebrin A	rat	EGFP	N-terminus	CMV	Tomoaki Shirao, (Gunma University) (Hayashi et al., 1996)	(Hayashi and Shirao, 1999; Biou et al., 2008)

Homer1b	rat	EGFP PAGFP	N-terminus N-terminus	CMV CMV	Shigetada Nakanishi (Osaka Bioscience Institute), Yoshiaki Tagawa (Kyoto University) (Hayashi et al., 2009) Baris Bingol, Morgan Sheng (MIT/Genentech)	(Sala et al., 2003; Hayashi et al., 2009)
Shank1b	rat	EGFP	N-terminus	CMV	Morgan Sheng (MIT/ Genentech), Carlo Sala (University of Milan) (Sala et al., 2001)	(Sala et al., 2003)
SAP97	rat	EGFP	N-terminus	CMV	Richard Huganir (Johns Hopkins) (Nakagawa et al., 2004b)	(Nakagawa et al., 2004b)
PSD-95	rat	EGFP	C-terminus	CAG	Shigeo Okabe (University of Tokyo) (Okabe et al., 1999)	(Okabe et al., 1999; Steiner et al., 2008)
α-actinin2	human	EGFP	C-terminus	CMV	Michael Ehlers (Duke/Pfizer) (Michailidis et al., 2007)	(Nakagawa et al., 2004a)

[1)] monomeric GFP: EGFP with A206K mutation (Zacharias et al., 2002).

SUPPLEMENTAL EXPERIMENTAL PROCEDURES

Hippocampal slice culture and gene transfection.

Animal experiments were conducted according to the MIT and RIKEN Committee for Animal Care guidelines. Hippocampal organotypic slice cultures were prepared from postnatal day 6-7 rats as described (Okamoto et al., 2004). Slices were cultured at 35 ºC on interface membranes (Millipore) and fed with MEM media containing 20% horse serum, 27 mM D-glucose, 6 mM $NaHCO_3$, 2 mM $CaCl_2$, 2 mM $MgSO_4$, 30 mM HEPES, 0.01 % ascorbic acid and 1 µg/ml insulin. pH was adjusted to 7.3 and osmolality to 300-320 mOsm. Slices were biolistically transfected (BioRad) after 5-7 DIV with a plasmid expressing RFP (DsRed2, Clontech) under CAG promoter and a plasmid expressing one of the GFP-fusion proteins (Table S1) or expressing EGFP alone. In cofilin replacement experiments, slices were transfected with two modified versions of the dual promoter FHUGW vector (Xu et al., 2008; kind gift from W. Xu): one where shRNA targeting ADF was expressed under H1 promoter and DsRed2 expressed under pUb promoter, and another one expressing shRNA targeting cofilin-1 (under H1) and shRNA-resistant versions of cofilin-GFP mutants (under pUb). Controls were done with empty H1 site (or with shRNA targeting Luciferase) and EGFP (under pUb) together with RFP plasmid. In Fig 6H, slices were transfected with pSuper expressing shRNA targeting LIMK1 and LIMK2 (Endo et al., 2007), cofilin-GFP and RFP (empty pSuper for Ctrl). Plasmids were either made in house or donated by the researchers cited in Table S1.

2P microscopy imaging and induction of sLTP in single spines.

Time-lapse fluorescence imaging was carried out with a 2P microscope (FluoView FV1000MPE, Olympus) equipped with two mode-lock femtosecond-pulse Ti:sapphire lasers (MaiTai HP, Sprectra-Physics). Slices were maintained at room temperature (r.t., 25-27°C) in a continuous perfusion of artificial cerebrospinal fluid (ACSF) containing 119 mM NaCl, 2.5 mM KCl, 3 mM $CaCl_2$, 26.2 mM $NaHCO_3$, 1 mM NaH_2PO_4 and 11 mM glucose, 1 µM tetrodotoxin, 50 µM picrotoxin and 6 mM 4-methoxy-7-nitroindolinyl (MNI)-L-glutamate (Tocris, Bristol, UK) equilibrated with 5% CO_2/95% O_2. Some of experiments were carried out at 2.5 mM MNI-glutamate with increased (4 mM) $CaCl_2$. Imaging was performed at 8-9 DIV in primary or secondary dendrites from the distal part of the main apical dendrite of CA1 pyramidal neurons. In order to avoid overexpression issues, we were particularly careful to select neurons with minimal GFP signal but bright enough to image above noise, with evident healthy dendritic morphology and no signs of fluorescent aggregates. At the end of each experiment we reconfirmed that the neuron kept its healthy dendritic morphology. We induced sLTP on thin or small mushroom spines, with clear head and neck. 2P uncaging of MNI-glutamate was performed at 720 nm and green and red fluorescence proteins were simultaneously excited at 910 nm. Both lasers were aligned daily by imaging and bleaching 0.5 µm fluorescent beads (Invitrogen). sLTP was induced by 1 ms pulses repeated at 1 Hz for 1 min aiming close to the tip of the spine, similarly to Matsuzaki et al. (2004). Laser intensity (3-5 mW) was adjusted for each experiment to obtain a stable spine volume increase of 50-100% for at least 30 min. These laser pulses triggered an averaged uEPSC response of 5.26 ± 0.94 pA, within a similar range to mini EPSC

responses from CA1 pyramidal neurons expressing GFP (n=18; gray trace in Fig. S1A) (De Simoni et al., 2003; Sala et al., 2003). For experiments involving photoactivation of PAGFP, 3 lasers were aligned: imaging was done using the confocal microscope mode of FV1000MPE at 488 nm excitation and dendrites close to the slice surface were selected. 2P glutamate uncaging was performed at 720 nm (as above) and PAGFP photoactivation at 820 nm by scanning the spine head for 500 ms (1-2 mW). Short-term cofilin-1 and Homer1b translocation experiments (Fig. 1A) were repeated at 30 °C and 35 °C, and long-term translocation of Homer1b experiment (Fig. 8B) was repeated at 30°C, both with similar results (data not shown).

Pharmacological reagents.

Tetrodotoxin (1 µM) was purchased from Latoxan (Valence, France), picrotoxin (50 µM) from Nacalai Tesque (Kyoto, Japan), U73122 (10 µM) and cycloheximide (60 µM) from Sigma-Aldrich, KN93 and KN62 (10 µM) from Enzo Lifescience (Plymouth Meeting, PA, USA), human BDNF (30 ng/ml) from Alomone Labs (Jerusalem, Israel), D-AP5 (100 µM), GSK429286 (10 µM), 2-methyl-6-(phenylethynyl)-pyridine (MPEP, 10 µM), and anisomycin (25 µM) from Tocris, and IPA3 (30 µM) from Calbiochem (Darmstadt, Germany).

Image analysis.

At every time-point, a series of 512 x 512 pixel XY-scanned images were taken every 1 µm of depth (Z). The fluorescence intensity of 7-10 of these images were summed to obtain a single image of collapse depth (Z-stacked). A constant region of

interest was outlined around the spine including the spine head and half of spine neck and the total integrated fluorescence intensity of the green and the red channels was calculated using ImageJ (by Rasband, W.S., U. S. National Institutes of Health). Values were background-subtracted and corrected for bleed-through and overall fluorescence fluctuations. We assumed that the spine volume and the amount of fusion protein were proportional to the integrated intensity of the RFP and the GFP signal, respectively (Svoboda, 2004). We confirmed that these values yielded similar results to those obtained from values of spine head area (data not shown). In Fig. 1-3, we only included those experiments showing >5% of spine enlargement at 20-30 min. In the rest of figures, all experiments were included. Spine surface area was calculated as the 2/3 power of the volume of a hypothetical sphere (Patterson et al., 2010). For analysis of the distribution of GFP-fused proteins within the spine head (Fig. 2, 4), a 60 x 5 pixel line was drawn across the spine head, centered on the peak of maximum RFP signal (i.e., the center of the spine), parallel (Fig. 2) or semi-perpendicular (Fig. 4) to the dendrite, and the green and red fluorescence intensity profiles were calculated. We fitted these profiles to a Gaussian curve using GraphPad Prism and calculated the full width at half maximum (FWHM). We inferred the unidimensional subspine protein distribution by comparing the widths of the green with the red intensity profiles (both normalized to their own peak value).

Immunohistochemistry after single spine glutamate uncaging sLTP.

Spines from EGFP-transfected neurons located close to the surface (10-40 μm) of organotypic slices were stimulated at different time points (from 1 to 80 min). Slices

were immediately fixed in 4% paraformaldehyde (PFA) in 0.1 M sodium phosphate buffer (PB; pH 7.4) at 4°C for 15 sec, microwaved for 10-15 sec at 700 mW (temperature up to 36-40°C), and kept in cold PFA for 4 min. Slices were then frozen in liquid N_2 for 15 sec and put back to PFA for 45 min at r.t or overnight at 4°C. These treatments improved the preservation of neuronal morphology and the antigenicity of slice cultures. Slices were blocked and permeabilized in 1% Triton, 2% bovine serum albumin (BSA) in PBS for 15 min, r.t., and incubated overnight at 4°C in 0.25% Triton/2% BSA/PBS with the following antibodies: rabbit anti-cofilin-1 (ab11062; 1:1000; or ab42824; 1:500; Abcam), rabbit anti-Homer1 (#160002; 1:500; SYSY) and rat anti-GFP (GF090R; 1:500; Nacalai Tesque). Secondary antibodies Alexa555 anti-rabbit and Alexa488 anti-rat (1:300) were used for 2 h at r.t. Images were taken with a confocal microscope (FV1000, Olympus). Average fluorescence, i.e., total immunofluorescence divided by spine area, was measured from stimulated and non-stimulated spines in the optimal optical section (where the signal in the spine head was maximal), in a blind fashion, and normalized to the average immunofluorescence of each whole optical section (to account for differences in staining across sections). Values were normalized to non-stimulated spines. Specificity of cofilin antibodies were confirmed by the lack of specific signal in brain sections from cofilin-1 knock-out mice (residual staining: 13.3 ± 3.2% of WT levels, likely due to glial and GABAergic cells; Rust et al., 2010) and by western blotting (Fig. S3A). Specificity of Homer1 antibody was confirmed by antigen preabsorption (residue 1-186 of human Homer1b, SYSY; residual staining: 8.2 ± 3.1%).

Induction of chemical LTP in dissociated cell culture and immunocytochemistry.

Hippocampal neurons were dissected from P0-1 rats, dissociated with 2 mg/ml papain (Worthington), and plated on poly-L-lysine (Sigma) coated 12 mm coverslips at a density of $5.3x10^4$ cells/cm^2 or coated plastic 35 mm wells at $4.0x10^5$ cells/cm^2. Neurons were maintained in NeurobasalA media supplemented with B27 and Glutamax (Invitrogen) and transfected using Lipofectamine 2000 (Invitrogen) with EGFP at 10-11 DIV. Chemical LTP was induced by glycine application in Mg^{2+}-free extracellular solution according to Fortin et al. (2010). Coverslips were incubated at r.t. with extracellular solution (in mM: 125 NaCl, 2.5 KCl, 2.0 $CaCl_2$, 33.0 D-glucose, 25.0 HEPES; pH was adjusted to 7.4 and osmolality to 300-310 mOsm/kg). After 20 min, glycine (200 µM), bicuculline (20 µM), strychnine (3 µM) and TTX (0.5 µM) were added for 10 min. Cells were then washed and incubated in the same extracellular solution but without glycine for 30 min. Cells were fixed with 4% PFA for 10 min and treated with methanol at -30 °C for 3 min. Immunocytochemistry was performed using rabbit anti-cofilin (ab11062; 1:1000; Abcam) or mouse anti-Homer1 (#160011; 1:200; SYSY) antibodies and imaged with a confocal microscope (FV1000, Olympus). Two dendritic segments of 50 µm per neuron, >5 neurons per experiment, 4 independent experiments, were analyzed in a blind fashion to the treatment. Immunofluorescence intensity was normalized by spine area.

Fluorescence lifetime imaging microscopy (FLIM).

Plasmid vector DNA encoding donor (cofilin-GFP) and acceptor (mRFP-actin, cofilin-mCherry, or mCherry) fluorescent proteins were cotransfected at 1:3 ratio.

Fluorescence lifetime was measured using time-correlated photon counting technology (SPC-730, Becker and Hickl and H7422P-40, Hamamatsu Photonics) at 910 nm excitation. Detection was synchronized with excitation light pulse using an external detector. Emission light was filtered with a 680 nm short-pass and 510 ± 35 nm band-pass filters. Bleed-through of the acceptor fluorescence into the emission channel was negligible. A Z-stack scanned at 0.7 μm separation was summed for analysis except for Fig. 5E-F, where only a single plane was scanned. Images were analyzed using a custom written macro in Igor Pro (Wavemetrics) and average fluorescent lifetime in the spine head was calculated (Lee et al., 2009; Murakoshi et al., 2011). Fluorescence lifetime was presented as the difference from the averaged baseline lifetime.

Electrophysiology.

Whole cell intracellular recordings were done in EGFP-transfected neurons, voltage clamped at -60 mV with a patch pipette (3-6 MΩ) containing 115 mM cesium methanesulfonate, 20 mM CsCl, 10 mM HEPES, 2.5 mM $MgCl_2$, 4 mM ATP disodium salt, 0.4 mM GTP trisodium salt, 10 mM sodium phosphocreatine, 0.6 mM EGTA, and 5 μM human non-muscle actin (Cytoskeleton; Sala et al., 2003; Tanaka et al., 2008). ACSF contained 1 mM $MgCl_2$ to isolate AMPAR component. We triggered uEPSC by uncaging MNI-glutamate with 2 ms pulses of 5 mW of 720 nm laser at 10 s interval. LTP was induced by pairing glutamate uncaging with 1 ms laser pulse for 60 times at 1 Hz while depolarizing cells at 0 mV (Matsuzaki et al., 2004). Peak amplitude was obtained by averaging 2 ms around the peak from 5 traces.

***In vitro* FRET experiments.**

His_6-YFP-actin was expressed in Sf9 cells using a pFastBac system (Invitrogen), purified using a Ni-sepharose column (Qiagen), and copolymerized with untagged human non-muscle actin (Cytoskeleton) at approximately 1:1 molar ratio in actin polymerization buffer (Cytoskeleton). Cofilin-CFP and -YFP were similarly expressed in Sf9 and used without further purification as they produce a major band on SDS-PAGE. Spectra were measured with a Photonic Multichannel Spectral Analyzer (Hamamatsu Photonics PMA-11) at 400 ± 7.5 nm excitation. At this excitation, direct excitation of YFP was negligible. To biochemically demonstrate binding between F-actin and cofilin, the mixture was centrifuged at 135,000 g for 30 min and supernatant (unbound) and pellet (bound) were recovered, separated on SDS-PAGE, and visualized by coomassie brilliant blue staining.

LIM kinase assay.

Hela cells were cotransfected with cofilin-GFP and either cofilin peptide 1-16 -mCherry or mCherry. Cells were serum starved for 3 hours and stimulated with epidermal growth factor (EGF, 100 ng/ml, Sigma) for 5 min at 37 ^{o}C. Cellular proteins were subjected to western blotting analysis using anti-phospho-S3 cofilin (1:1000, Cell signal), anti-GFP (1:1000, Invitrogen), and anti-mCherry (1:1000, Clontech) antibodies. Band intensities were quantified using ImageJ (NIH).

Correlated 2P and EM imaging.

For a given neuron, a straight segment of a dendrite, located parallel to the slice surface was selected and up to three spines were stimulated at different positions and at

different time points (separated at least by >10 µm in space or >20 min in time). After the stimulation of the last spine, the slice was fixed with 2% PFA and 2% glutaraldehyde in PB for 90 min at r.t. and then for a minimum of 12 hours at 4ºC. Slices were subsequently rinsed thoroughly in PB, transferred to another 2P microscope chamber and perfused continuously with ice-cold 0.1 M Tris-HCl (pH 7.4) solution containing 1.5 mg/ml of diaminobenzidine (DAB), bubbled with pure oxygen. We localized the same dendritic region and photo-precipitated DAB by line-scanning the tissue with the 720 nm 2P laser, similarly to Tanaka et al. (2005). Different sets of lines were drawn and used as landmarks for EM analysis, including 2 lines flanking the dendrite in parallel, 3 lines pointing semi-perpendicularly to the stimulated spines, and 2 oblique lines located several microns above the dendrite (Fig. 7B). Slices were then transferred to PB, exposed for 30 min to 1% osmium tetroxide and 1.5% potassium ferrocyanide, another 30 min to 1% osmium tetroxide alone and then serially dehydrated in alcohol for flat-embedding between two sheets of ACLAR (Honeywell, Allied Signal, Morristown) with Durcupan epoxic resin (Sigma-Aldrich). After 2 days of curing at 57 ºC the samples were glued with Araldite on Durcupan BEEM cylinders and cut with a 45º Cryotrim diamond knife (Diatome, Biel, Switzerland) for block trimming. Semi-thin sections (500 nm) were obtained with a glass knife and stained with 1% of toluidine blue until the appearance of DAB marks was seen. At this point, we initiated the serial sectioning of the sample at 70 nm thickness with a 35º diamond knife (Diatome). Sections were mounted onto 1% Pioloform coated SynapTek slotted grids, 23000X EM images were taken with an FEI Tecnai Spirit TEM (FEI, Hillsboro) and merged to form a collage. Image alignment, reconstruction and analysis were done with the Reconstruct software package (Fiala,

2005). We reconstructed the same type of stimulated and unstimulated spines, i.e., thin or mushroom spines, not stubby or filopodia, in a blind way. Theoretical changes in neck resistance (R) were estimated by approximating the spine neck to a cylinder and calculating R=L/A, where L is the cylinder length and A the open cross-section area.

Statistical analyses.

All values are expressed as mean ± SEM (standard error of the mean). Statistical significance was set at the 95% confidence level (two tailed) and calculated using GraphPad Prism. Normality was analyzed using Kolmogorov-Smirnov test. Repeated measures ANOVA followed by *post hoc* paired Student's t-test was used to calculate differences between the average of the 20-30 min interval and the baseline in Fig. 1A, S1A, S2A-B. Repeated measures ANOVA followed by Dunnett's *post hoc* test was used to calculate differences between each time point and the corresponding baseline or control in Fig. 2A-B, I, Fig. 4A5, B5, C5, Fig. 5C-D, F, H-I, K-L, Fig. 8B, D-E, Fig. S2E-G, I-J, Fig. S6B, D. Student's paired *t*-test was used to calculate differences in bound fraction and fast and slow time constants in Fig. 4A3, B3, C3. One-way ANOVA followed by Student's *t*-test was used in Fig. 2C, G-H, Fig. 3C, E-F, Fig. 6B, E-F, O-P, Fig. S1B-E, Fig. S5A-C, G-I, and Fig. S6E. One-way ANOVA followed by Newman-Keuls *post hoc* test was used in Fig. 7I-K. Wilcoxon rank sum test was used in Fig. S5J-K. Pharmacological or genetic experiments were statistically compared to their corresponding vehicle or wild type controls and experiments were performed in an interleaved way, each one in a different slice but within the same experimental day. The order of control and experimental conditions were randomly swapped. Each "n" equals one stimulated (or unstimulated) spine. Typically, two spines per slice were stimulated,

either on the same neuron but in different dendrites, or in a different neuron in the same slice. In Fig. 1B, three spines per slice were stimulated. In Fig. 3E-F, each “n” equals one neuron.

SUPPLEMENTAL REFERENCES

Ackermann, M., and Matus, A. (2003). Activity-induced targeting of profilin and stabilization of dendritic spine morphology. Nat Neurosci *6*, 1194-1200.

Aizawa, H., Wakatsuki, S., Ishii, A., Moriyama, K., Sasaki, Y., Ohashi, K., Sekine-Aizawa, Y., Sehara-Fujisawa, A., Mizuno, K., Goshima, Y., *et al.* (2001). Phosphorylation of cofilin by LIM-kinase is necessary for semaphorin 3A-induced growth cone collapse. Nat Neurosci *4*, 367-373.

Asrican, B., Lisman, J., and Otmakhov, N. (2007). Synaptic strength of individual spines correlates with bound Ca2+-calmodulin-dependent kinase II. J Neurosci *27*, 14007-14011.

Biou, V., Brinkhaus, H., Malenka, R.C., and Matus, A. (2008). Interactions between drebrin and Ras regulate dendritic spine plasticity. Eur J Neurosci *27*, 2847-2859.

De Simoni, A., Griesinger, C.B., and Edwards, F.A. (2003). Development of rat CA1 neurones in acute versus organotypic slices: role of experience in synaptic morphology and activity. J Physiol *550*, 135-147.

Di Nardo, A., Gareus, R., Kwiatkowski, D., and Witke, W. (2000). Alternative splicing of the mouse profilin II gene generates functionally different profilin isoforms. J Cell Sci *113*, 3795-3803.

Endo, M., Ohashi, K., and Mizuno, K. (2007). LIM kinase and slingshot are critical for neurite extension. J Biol Chem *282*, 13692-13702.

Fiala, J.C. (2005). Reconstruct: a free editor for serial section microscopy. J Microsc *218*, 52-61.

Fischer, M., Kaech, S., Knutti, D., and Matus, A. (1998). Rapid actin-based plasticity in dendritic spines. Neuron *20*, 847-854.

Fortin, D.A., Davare, M.A., Srivastava, T., Brady, J.D., Nygaard, S., Derkach, V.A., and Soderling, T.R. (2010). Long-term potentiation-dependent spine enlargement requires synaptic Ca^{2+}-permeable AMPA receptors recruited by CaM-kinase I. J Neurosci *30*, 11565-11575.

Gu, J., Lee, C.W., Fan, Y., Komlos, D., Tang, X., Sun, C., Yu, K., Hartzell, H.C., Chen, G., Bamburg, J.R., *et al.* (2010). ADF/cofilin-mediated actin dynamics regulate AMPA receptor trafficking during synaptic plasticity. Nat Neurosci *13*, 1208-1215.

Hayashi, K., Ishikawa, R., Ye, L.H., He, X.L., Takata, K., Kohama, K., and Shirao, T. (1996). Modulatory role of drebrin on the cytoskeleton within dendritic spines in the rat cerebral cortex. J Neurosci *16*, 7161-7170.

Hayashi, K., and Shirao, T. (1999). Change in the shape of dendritic spines caused by overexpression of drebrin in cultured cortical neurons. J Neurosci *19*, 3918-3925.

Hayashi, M.K., Tang, C., Verpelli, C., Narayanan, R., Stearns, M.H., Xu, R.M., Li, H., Sala, C., and Hayashi, Y. (2009). The postsynaptic density proteins Homer and Shank form a polymeric network structure. Cell *137*, 159-171.

Johnston, S.A., Bramble, J.P., Yeung, C.L., Mendes, P.M., and Machesky, L.M. (2008). Arp2/3 complex activity in filopodia of spreading cells. BMC Cell Biol *9*, 65.

Kopec, C.D., Li, B., Wei, W., Boehm, J., and Malinow, R. (2006). Glutamate receptor exocytosis and spine enlargement during chemically induced long-term potentiation. J Neurosci *26*, 2000-2009.

Lee, S.J., Escobedo-Lozoya, Y., Szatmari, E.M., and Yasuda, R. (2009). Activation of CaMKII in single dendritic spines during long-term potentiation. Nature *458*, 299-304.
Makino, H., and Malinow, R. (2009). AMPA receptor incorporation into synapses during LTP: the role of lateral movement and exocytosis. Neuron *64*, 381-390.
Maldonado, M. (2010). Arp2/3 complex has a neuroprotective role and is required for mature dendritic spine head morphology. In The faculty of the graduate school (The University of Minnesota).
Matsuzaki, M., Honkura, N., Ellis-Davies, G.C., and Kasai, H. (2004). Structural basis of long-term potentiation in single dendritic spines. Nature *429*, 761-766.
Michailidis, I.E., Helton, T.D., Petrou, V.I., Mirshahi, T., Ehlers, M.D., and Logothetis, D.E. (2007). Phosphatidylinositol-4,5-bisphosphate regulates NMDA receptor activity through α-actinin. J Neurosci *27*, 5523-5532.
Murakoshi, H., Wang, H., and Yasuda, R. (2011). Local, persistent activation of Rho GTPases during plasticity of single dendritic spines. Nature *472*, 100-104.
Nakagawa, T., Engler, J.A., and Sheng, M. (2004a). The dynamic turnover and functional roles of alpha-actinin in dendritic spines. Neuropharmacology *47*, 734-745.
Nakagawa, T., Futai, K., Lashuel, H.A., Lo, I., Okamoto, K., Walz, T., Hayashi, Y., and Sheng, M. (2004b). Quaternary structure, protein dynamics, and synaptic function of SAP97 controlled by L27 domain interactions. Neuron *44*, 453-467.
Okabe, S., Kim, H.D., Miwa, A., Kuriu, T., and Okado, H. (1999). Continual remodeling of postsynaptic density and its regulation by synaptic activity. Nat Neurosci *2*, 804-811.
Okamoto, K., Nagai, T., Miyawaki, A., and Hayashi, Y. (2004). Rapid and persistent modulation of actin dynamics regulates postsynaptic reorganization underlying bidirectional plasticity. Nat Neurosci *7*, 1104-1112.
Patterson, M.A., Szatmari, E.M., and Yasuda, R. (2010). AMPA receptors are exocytosed in stimulated spines and adjacent dendrites in a Ras-ERK-dependent manner during long-term potentiation. Proc Natl Acad Sci USA *107*, 15951-15956.
Rust, M.B., Gurniak, C.B., Renner, M., Vara, H., Morando, L., Görlich, A., Sassoè-Pognetto, M., Banchaabouchi, M.A., Giustetto, M., Triller, A., *et al.* (2010). Learning, AMPA receptor mobility and synaptic plasticity depend on n-cofilin-mediated actin dynamics. EMBO J *29*, 1889-1902.
Sala, C., Futai, K., Yamamoto, K., Worley, P.F., Hayashi, Y., and Sheng, M. (2003). Inhibition of dendritic spine morphogenesis and synaptic transmission by activity-inducible protein Homer1a. J Neurosci *23*, 6327-6337.
Sala, C., Piech, V., Wilson, N.R., Passafaro, M., Liu, G., and Sheng, M. (2001). Regulation of dendritic spine morphology and synaptic function by Shank and Homer. Neuron *31*, 115-130.
Saneyoshi, T., Wayman, G., Fortin, D., Davare, M., Hoshi, N., Nozaki, N., Natsume, T., and Soderling, T.R. (2008). Activity-dependent synaptogenesis: regulation by a CaM-kinase kinase/CaM-kinase I/βPIX signaling complex. Neuron *57*, 94-107.
Shen, K., Teruel, M.N., Subramanian, K., and Meyer, T. (1998). CaMKIIβfunctions as an F-actin targeting module that localizes CaMKIIα/βheterooligomers to dendritic spines. Neuron *21*, 593-606.
Shi, S.H., Hayashi, Y., Petralia, R.S., Zaman, S.H., Wenthold, R.J., Svoboda, K., and Malinow, R. (1999). Rapid spine delivery and redistribution of AMPA receptors after synaptic NMDA receptor activation. Science *284*, 1811-1816.

Steiner, P., Higley, M.J., Xu, W., Czervionke, B.L., Malenka, R.C., and Sabatini, B.L. (2008). Destabilization of the postsynaptic density by PSD-95 serine 73 phosphorylation inhibits spine growth and synaptic plasticity. Neuron *60*, 788-802.
Svoboda, K. (2004). Do spines and dendrites distribute dye evenly? Trends Neurosci *27*, 445-446.
Syriani, E., Gomez-Cabrero, A., Bosch, M., Moya, A., Abad, E., Gual, A., Gasull, X., and Morales, M. (2008). Profilin induces lamellipodia by growth factor-independent mechanism. FASEB J *22*, 1581-1596.
Tada, T., Simonetta, A., Batterton, M., Kinoshita, M., Edbauer, D., and Sheng, M. (2007). Role of Septin cytoskeleton in spine morphogenesis and dendrite development in neurons. Curr Biol *17*, 1752-1758.
Tanaka, J., Horiike, Y., Matsuzaki, M., Miyazaki, T., Ellis-Davies, G.C., and Kasai, H. (2008). Protein synthesis and neurotrophin-dependent structural plasticity of single dendritic spines. Science *319*, 1683-1687.
Tanaka, J., Matsuzaki, M., Tarusawa, E., Momiyama, A., Molnar, E., Kasai, H., and Shigemoto, R. (2005). Number and density of AMPA receptors in single synapses in immature cerebellum. J Neurosci *25*, 799-807.
Xu, W., Schluter, O.M., Steiner, P., Czervionke, B.L., Sabatini, B., and Malenka, R.C. (2008). Molecular dissociation of the role of PSD-95 in regulating synaptic strength and LTD. Neuron *57*, 248-262.
Zacharias, D.A., Violin, J.D., Newton, A.C., and Tsien, R.Y. (2002). Partitioning of lipid-modified monomeric GFPs into membrane microdomains of live cells. Science *296*, 913-916.
Zhang, Y.P., Holbro, N., and Oertner, T.G. (2008). Optical induction of plasticity at single synapses reveals input-specific accumulation of α CaMKII. Proc Natl Acad Sci USA *105*, 12039-12044.